OPTICS SOLUTIONS FOR THE COLLIMATION INSERTIONS OF LHC

D.I.Kaltchev, M.K.Craddock[1], TRIUMF, 4004 Wesbrook Mall, Vancouver, B.C., Canada V6T2A3
J.B.Jeanneret, A.Verdier, CERN, CH-1211 Geneva 23, Switzerland

Abstract

While the two collimation insertions in the LHC must have similar basic layouts and match to almost identical dispersion suppressors to respect the geometry of the existing tunnel, their different roles impose opposite requirements on the normalized dispersion within them. For betatron collimation it must be near zero, while for momentum collimation it must have a peak at the location of the primary collimator, immediately after the dispersion suppressor. The insertion lattice solution found for the latter case requires up to 30% asymmetry in the quadrupole gradients (in line with the current trend in LHC lattice development to break the exact antisymmetry within insertions). To achieve this using twin-aperture warm quadrupoles, the modules making up each quadrupole will be wired in such a way that the two beams still see the same sequence of focusing fields. We describe the optimum setup, flexibility and collimation quality for the two insertions.

1 INTRODUCTION

In the LHC, composed of superconducting magnets in which proton beams of both high energy and high current will be stored, the local power deposition associated with beam losses will be larger than the magnet quench level by several orders of magnitude [1],[2]. In addition the large size of the ring and the need for high magnetic field requires keeping the geometrical aperture (defined by the vacuum chamber) to a bare minimum. Not far outside the dynamic aperture the transverse motion of the particles becomes chaotic and can form a primary halo diffusing towards the geometrical aperture. The transverse extent of the halo is kept below the chaotic limit by absorbing these protons in primary collimators made of metallic blocks, called jaws below. At all energies proton absorption in the primary jaws is far from complete [2]. Protons which are not absorbed may be scattered elastically off the jaw, thus forming a secondary halo which can also induce quenches. Secondary jaws are therefore necessary to limit the extent of the secondary halo to a value smaller than the geometrical aperture. In the LHC, both betatron and momentum collimation are needed.

For colliding beams, beam-beam induced non-linearities, combined with residual magnetic imperfections of the quadrupoles in the experimental insertions, limit the dynamic aperture to $A_{dyn} \sim$ 6–10 in units of σ_β, the rms beam radius. The flux of protons diffusing outside this amplitude is estimated to be $\dot{n} \sim 3 \times 10^9\ \mathrm{p\,s^{-1}}$ [1]. Most of these protons might touch the vacuum chamber at a single aperture limit, with the energy release spread longitudinally by the hadronic shower process over $l_{shower} \approx 1$ m. In these conditions the local quench level is reached with $\dot{n}_q \sim 10^6\ \mathrm{p\,s^{-1}m^{-1}}$[2]. At ramping, rf-untrapped protons are not accelerated and migrate slowly towards the vacuum chamber. The flash of losses lasts $\Delta t \leq 1$ s, a time scale fixing the transient quench level at $\Delta n_q = 2.5\ 10^{10}\ \mathrm{p\,m^{-1}}$. For a stored intensity $N_p = 3\ 10^{14}$ protons with 5% off-bucket, the intensity of the flash is $\Delta n = 1.5\ 10^{13}$ p [2].

A very efficient collimation system is therefore needed in both cases. It has been shown [2] that two–stage collimation is adequate and offers a good safety margin.

2 REQUIREMENTS FOR THE OPTICS

2.1 Betatron collimation

With an approximately circular normalized aperture, the primary halo must be intercepted by three primary jaws forming an octagonal primary aperture of inscribed radius n_1. It is shown in [3] that the secondary halo can be cut close to the secondary collimator aperture $A_{sec} = n_2$ if, for each primary, four secondary jaws are installed at well-defined correlated betatronic phase advances μ_x and μ_y relative to the primary jaws. The long straight sections of LHC offer a phase advance $\Delta\mu_{x,y} \approx 2\pi$, which proved to be insufficient to satisfy the ideal phase conditions for the twelve secondary jaws. With the code DJ [4][5], various optics were studied, the present best result for a ratio $n_2/n_1 = 7/6$ being $A_{sec} = 1.2n_2 = 1.4n_1$. With a ring aperture $A_{ring} = 10$ (including tolerances, optical errors and momentum spread) and using the safe condition $A_{sec} < A_{ring}$, the allowed primary aperture is therefore $n_1 \leq A_{ring}/1.4 = 7.1$, a value which is adequate at both injection and collision beam energies.

2.2 Momentum collimation

In contrast to the betatron halo, which may drift away from the beam in all transverse directions, momentum losses in a ring with only horizontal dispersion are concentrated in the horizontal plane. Off-bucket protons lost at ramping keep their initial betatron amplitude [6] and are therefore confined in the range of betatron amplitudes $A_{x,y} \approx 2$. It is therefore sufficient to use a single horizontal primary collimator, with its four associated secondary collimators. Their phase advances relative to the primary jaw are given in Table 1 [3]. With the largest momentum offset passing the primary jaw $\delta_c = n_1/\chi_1$ (where the normalized dispersion $\chi_1 = D_1/\sqrt{\epsilon\beta}$), the secondaries limit the horizontal betatron amplitude to $\approx \sqrt{n_2^2 - n_1^2}$. In the arc of a ring, the aperture limit for a particle with momentum offset is located near horizontally focusing quadrupoles, where both

[1] Also at Dept. of Physics & Astronomy, UBC, Vancouver, Canada.

β_x and D_x are at their maximum. The largest horizontal excursions of the secondary halo must fit the arc aperture, i.e. $A_{x,\beta} + D\delta_p = N_{x,arc}$.

The smaller number of correlated phase advances for the secondary collimators makes solution easier than in the betatronic case, but a large normalized dispersion χ_1 (or $\eta_1 = D_1/\sqrt{\beta}$) is needed at the primary collimator. The value of η_1 depends mainly on the ring aperture $A_{ring}(\delta_p = 0)$and on the maximum dispersion η_{arc}. We use [3]

$$\eta_1(n_1) = \frac{n_1 \eta_{arc}}{A_{ring}(\delta_p = 0) - (n_2^2 - n_1^2)^{1/2}}. \quad (1)$$

In LHC, with $A_{ring}(\delta_p = 0) = 12$, $\eta_{arc} = 0.2\,\mathrm{m}^{1/2}$ (with optical errors) and $n_1 = 7$, $\eta_1 = 0.19\,\mathrm{m}^{1/2}$ is needed [7]. The geometry of the dispersion suppressor connecting the arcs and the straight section is fixed by the existing tunnel and therefore offers little flexibility for altering the dispersion function in the insertion, which is suppressed for the nominal tune. The combination of dispersion and phase constraints therefore requires a lot of flexibility in the straight section itself where the quadrupoles can be located with more freedom.

Table 1: Secondary collimator locations μ_x and μ_y relative to the horizontal primary jaw of the momentum cleaning insertion and their X–Y azimuthal orientations α_{Jaw}. The angle ϕ is the scattering angle (projected on to the XY plane) for which the secondary does the most efficient cut; $\mu_0 = \arccos(n_1/n_2)$.

ϕ	μ_x	μ_y	α_{Jaw}
0	μ_o	-	0
π	$\pi - \mu_o$	-	0
$\pi/2$	π	$3\pi/2$	μ_o
$-\pi/2$	π	$3\pi/2$	-μ_o

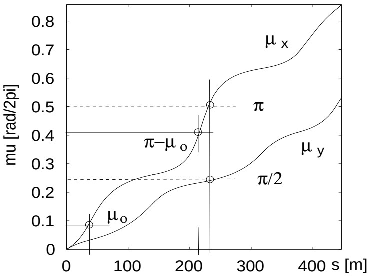

Figure 1: The phase advances along the momentum cleaning insertion relative to the location of the primary collimator. The three vertical marks indicate the optimum phase advances of Table 1.

3 COLLIMATION INSERTION LATTICES

So that the two beams in the LHC experience exactly the same sequence of focusing fields in a FODO lattice composed of twin-aperture quadrupoles, these are arranged left-right (L-R) antisymmetrically about the midpoint of each insertion. Thus the six straight-section quadrupoles QiL, QiR (i=4,5,6 - see Fig. 2 (top)) nominally have gradients $K_i^L = -K_i^R$. This condition was found too restrictive

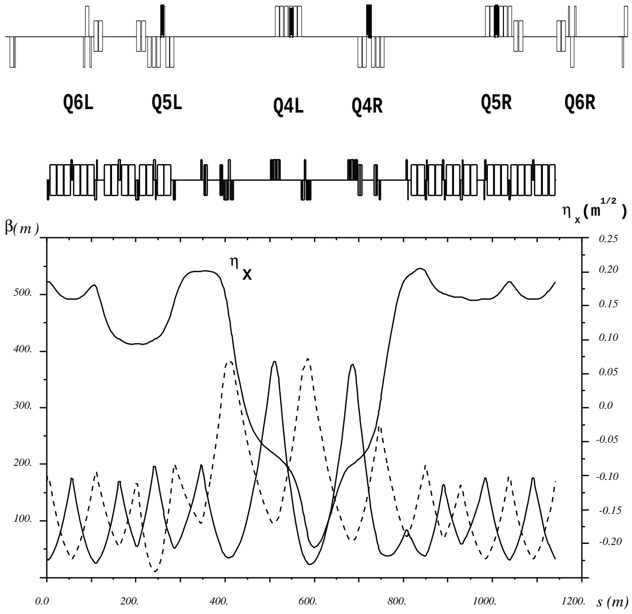

Figure 2: Momentum cleaning insertion lattice. Top: straight section layout. Bottom: beta functions and normalized dispersion.

for both betatron and momentum collimation, and so new optics have been devised for the cleaning insertions whose basic feature is to give the quadrupoles an increased left-right symmetric component $K_i^S = (K_i^L + K_i^R)/2$. Other changes from the optics reported in [8] include replacement of the strongest warm quadrupoles Q6L and R by cold quadrupole groups, and repositioning of the separation magnets and the primary jaws to a new location between Q6L and Q5L. The latter allows neutral and low-momentum charged particles to be removed from the beam axis more efficiently.

3.1 *Momentum collimation*

The advantages of the new optics over an exactly antisymmetric setting are that they allow: (1) lower over-all focusing strengths, both for the straight section and dispersion suppressor quadrupoles, and (2) a higher normalized dispersion peak at the primary collimator, η_x=0.19-0.22 (Fig. 2, bottom), as momentum collimation requires. The suggested explanation for this is that with antisymmetry broken, the Twiss function values at the symmetry point can be set further away from the exact antisymmetry condition $\beta^{*L}_{x,y} = \beta^{*R}_{y,x}$, $\alpha^{*L}_{x,y} = -\alpha^{*R}_{y,x}$ (this condition was never forced as a constraint). With $K_i^L = -K_i^R$ (i=4,5,6), the best result for the normalized dispersion was $\eta_x = 0.16$ [8].

The four quadrupoles QiL and QiR (i=4,5) are in fact each composed of 6 warm quadrupole modules 3 m long, based on the “two channels in one bore” design concept [1]. Normally, these modules are wired so that the fields felt by the two beams are exactly reversed, one seeing an F quadrupole, and the other a D (as assumed for the antisymmetric lattice described above). Small deviations from equal powering of the two channels are possible, but are

Table 2: Quadrupole gradients (as % of maximum allowed) and normalized dispersion at the primary collimator for the momentum cleaning insertion matched to four arc cell tunes

$\nu_x^{a.cell}$	.2515	.2649	.28	.24
$\nu_y^{a.cell}$	.2401	.2377	.24	.20
K_4^A	81	84	84	83
K_4^S	54	49	50	57
K_5^A	-88	-86	-86	86
K_5^S	70	46	62	61
K_6^L	80	83	-74	-75
K_6^R	-74	-75	83	81
K_i^L	73	-17	55	39
for left	83	66	43	96
dispersion	45	38	71	25
suppressor	11	10	-5.5	21
and	-67	-81	-80	-1
2 arc trim	-25	-11	-29	8
quadrupoles	-14	-76	-63	-92
K_i^R	-75	-93	90	-95
for right	68	-74	-82	84
dispersion	-74	-67	-51	-62
suppressor	53	-47	12	-13
and	-7	20	3.5	20
2 arc trim	74	15	52	9
quadrupoles	4	-58	12	-23
η_x at prim. $[\mathrm{m}^{1/2}]$	.2	.18	.194	.194
$d\eta_x/d\mu_x$ $[\mathrm{m}^{1/2}]$	-.012	-.042	-.039	-.010

limited to $10 - 15\%$, for reasons of field quality.

To achieve larger $|(K_i^L + K_i^R)/K_i^R|$ ($\sim 30\%$ is needed), while preserving identical straight-section optics for the two beams and also good field quality in the warm modules, a second kind of module is introduced, wired so that each beam sees the same field, both channels acting as F quadrupoles. These new "symmetric" modules (solid black in Fig. 2) are positioned near the middle of each quadrupole assembly, where they are most effective.

3.2 Matching and Flexibility

The cleaning insertions were matched to the arcs using MAD [9] with a total of 21 independent variables: 18 quadrupole strengths (2 K_i^S for the symmetric modules, 2 K_i^A for the antisymmetric ones, 2 for the cold Q6L and R, and 12 for the dispersion suppressor (DS) trims) plus the 3 positions of the straight-section quadrupoles. The most important constraint was the need for a maximum flat-topped dispersion peak at the primary collimator. Table 2 shows the quadrupole strengths needed to match the momentum cleaning insertion to the arcs, while optimizing the normalized dispersion η_x and its derivative $d\eta_x/d\mu_x = (\alpha_x D_x + \beta_x D_x')/\sqrt{\beta_x}$. Four cases are shown, for different tunes of the arc cells: the first column is for the nominal tune, while the other three assure cancellation of various nonlinear resonance driving terms. The tune advances for the nominal case are shown on Figure 1. For all four cases the quadrupole strengths are within limits, η_x is sufficiently high and $|d\eta_x/d\mu_x|$ is sufficiently small.

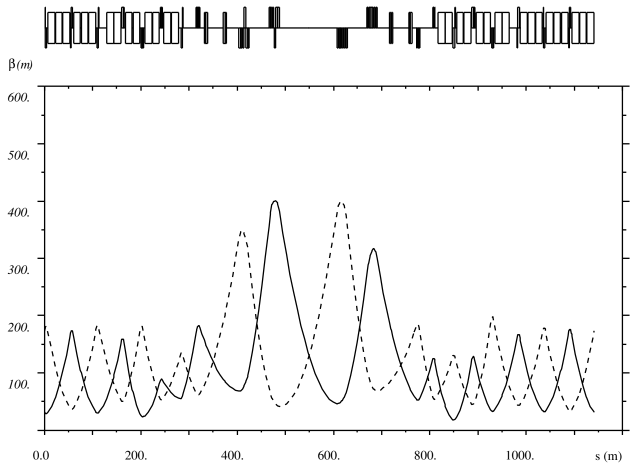

Figure 3: Betatron cleaning insertion lattice.

3.3 Betatron collimation

The betatron cleaning section (Figure 3) has in general preserved the optics described in [5]. As for momentum cleaning, symmetrically powered quadrupole modules help to increase flexibility and reduce quadrupole strengths.

4 CONCLUSIONS

By using the two-in-one warm quadrupoles of the collimation insertions in a flexible way, we have formulated a two-stage momentum cleaning insertion which satisfies the LHC machine requirements and which is also, to our knowledge, the first fully worked out design for any machine.

5 REFERENCES

[1] *Large Hadron Collider*, CERN/AC/95-05(LHC) (1995).

[2] N. Catalan Lasheras, G. Ferioli, J.B. Jeanneret, R. Jung, D.I. Kaltchev and T. Trenkler, *Proc. Symp. Near Beam Physics, Fermilab, 1997*, edited by D. Carrigan and N. Mokhov, p. 117, and CERN LHC Project Report 156 (1998).

[3] J.B. Jeanneret, Phys. Rev. ST Accel. Beams, **1**, 081001 (1998).

[4] D.I. Kaltchev, M.K. Craddock, R.V. Servranckx and J.B. Jeanneret, *Proc. EPAC96, Sitges, 1996*, ed. S. Myers et al., p. 1432 (IOP, 1996); CERN LHC Project Report 37 (1996).

[5] D.I. Kaltchev, M.K. Craddock, R.V. Servranckx and J.B. Jeanneret, *Proc. PAC'97, Vancouver*, ed. M. Comyn et al., p. 153 (IEEE, 1998); CERN LHC Proj. Rept. 134 (1997).

[6] N. Catalan Lasheras, CERN LHC Proj. Rept. 200 (1998).

[7] J.B. Jeanneret, CERN LHC Project Note 115 (1997).

[8] D.I. Kaltchev, M.K. Craddock, R.V. Servranckx and T. Risselada,*Proc. EPAC98, Stockholm,* p. 353 (IOP, 1998).

[9] H. Grote and F.C. Iselin. *MAD Program Version 8.16, User's Reference Manual*, CERN/SL/90-13(AP) (1995).